

Lawrence Berkeley National Laboratory

LBL Publications

Title

Deforestation reshapes land-surface energy-flux partitioning

Permalink

<https://escholarship.org/uc/item/9hb4612w>

Journal

Environmental Research Letters, 16(2)

ISSN

1748-9318

Authors

Yuan, Kunxiaoja
Zhu, Qing
Zheng, Shiyu
[et al.](#)

Publication Date

2021-02-01

DOI

10.1088/1748-9326/abd8f9

Peer reviewed

LETTER • OPEN ACCESS

Deforestation reshapes land-surface energy-flux partitioning

To cite this article: Kunxiaoia Yuan *et al* 2021 *Environ. Res. Lett.* **16** 024014

View the [article online](#) for updates and enhancements.

ENVIRONMENTAL RESEARCH
LETTERS

LETTER

Deforestation reshapes land-surface energy-flux partitioning

Kunxiaoja Yuan^{1,2} , Qing Zhu² , Shiyu Zheng³, Lei Zhao⁴ , Min Chen^{5,6}, William J Riley², Xitian Cai² , Hongxu Ma⁷, Fa Li^{1,2} , Huayi Wu¹ and Liang Chen⁸

OPEN ACCESS

RECEIVED
15 July 2020REVISED
1 December 2020ACCEPTED FOR PUBLICATION
6 January 2021PUBLISHED
21 January 2021Original content from
this work may be used
under the terms of the
[Creative Commons
Attribution 4.0 licence](#).Any further distribution
of this work must
maintain attribution to
the author(s) and the title
of the work, journal
citation and DOI.

- ¹ State Key Laboratory of Information Engineering in Surveying, Mapping and Remote Sensing, Wuhan University, Wuhan, Hubei, People's Republic of China
- ² Climate and Ecosystem Sciences Division, Climate Sciences Department, Lawrence Berkeley National Laboratory, Berkeley, CA, United States of America
- ³ School of Electrical Engineering, Tsinghua University, Beijing, People's Republic of China
- ⁴ Department of Civil and Environmental Engineering, University of Illinois Urbana-Champaign, Champaign, IL, United States of America
- ⁵ Joint Global Change Research Institute, Pacific Northwest National Laboratory, College Park, MD, United States of America
- ⁶ Department of Forest and Wildlife Ecology, University of Wisconsin-Madison, Madison, WI, United States of America
- ⁷ Department of Geography, University of California, Berkeley, CA, United States of America
- ⁸ Illinois State Water Survey, University of Illinois at Urbana-Champaign, Champaign, IL, United States of America

E-mail: qzhu@lbl.gov and kunxiaojiayuan@lbl.gov**Keywords:** climate change, deforestation, cause–effect relationship, earth system modelSupplementary material for this article is available [online](#)**Abstract**

Land-use and land-cover change significantly modify local land-surface characteristics and water/energy exchanges, which can lead to atmospheric circulation and regional climate changes. In particular, deforestation accounts for a large portion of global land-use changes, which transforms forests into other land cover types, such as croplands and grazing lands. Many previous efforts have focused on observing and modeling land–atmosphere–water/energy fluxes to investigate land–atmosphere coupling induced by deforestation. However, interpreting land–atmosphere–water/energy-flux responses to deforestation is often complicated by the concurrent impacts from shifts in land-surface properties versus background atmospheric forcings. In this study, we used 29 paired FLUXNET sites, to improve understanding of how deforested land surfaces drive changes in surface-energy-flux partitioning. Each paired sites included an intact forested and non-forested site that had similar background climate. We employed transfer entropy, a method based on information theory, to diagnose directional controls between coupling variables, and identify nonlinear cause–effect relationships. Transfer entropy is a powerful tool to detective causal relationships in nonlinear and asynchronous systems. The paired eddy covariance flux measurements showed consistent and strong information flows from vegetation activity (gross primary productivity (GPP)) and physical climate (e.g. shortwave radiation, air temperature) to evaporative fraction (EF) over both non-forested and forested land surfaces. More importantly, the information transfers from radiation, precipitation, and GPP to EF were significantly reduced at non-forested sites, compared to forested sites. We then applied these observationally constrained metrics as benchmarks to evaluate the Energy Exascale Earth System Model (E3SM) land model (ELM). ELM predicted vegetation controls on EF relatively well, but underpredicted climate factors on EF, indicating model deficiencies in describing the relationships between atmospheric state and surface fluxes. Moreover, changes in controls on surface energy flux partitioning due to deforestation were not detected in the model. We highlight the need for benchmarking model simulated surface–energy fluxes and the corresponding causal relationships against those of observations, to improve our understanding of model predictability on how deforestation reshapes land surface energy fluxes.

1. Introduction

The land surface and atmosphere are closely coupled through energy, water, and carbon cycles (Santanello *et al* 2013, Gentine *et al* 2019). For example, the land surface dissipates energy and water into the atmosphere through evapotranspiration and latent heat fluxes. Plants open stomata to receive atmospheric CO₂ and produce carbohydrates, which simultaneously lose water through transpiration (Lei *et al* 2010, Suyker and Verma 2010). The dissipated latent heat and evapotranspiration fluxes modulate atmospheric temperature and water vapor pressure, which in return can affect vegetation and soil processes (Allison and Treseder 2011, Lombardozzi *et al* 2015). The strengths of such two-way interactions between land and atmosphere are strongly dependent on land-surface characteristics (e.g. soil temperature, wetness) (Dirmeyer 2011, Ford *et al* 2014, Feldman *et al* 2019), and atmospheric conditions (e.g. vapor pressure deficit (VPD), radiation, and air temperature) (Zhang *et al* 2014, Zhou *et al* 2014, Kukal and Irmak 2016). Moreover, land–atmosphere interactions are largely mediated by local vegetation (e.g. grass or tree) and exhibit complex energy, water, and carbon coupling among the soil, the vegetation, and the atmosphere (Puma *et al* 2013, Williams and Torn 2015).

To better understand the land–atmosphere coupling that includes the whole soil-vegetation-atmosphere continuum, two segments of this coupling are commonly distinguished: (a) the land segment, i.e. the linkage between land states (e.g. soil moisture) and surface energy flux patterns (e.g. latent heat flux) and (b) the atmosphere segment, i.e. the relationship between surface-energy flux patterns and atmospheric states (e.g. precipitation) (Guo *et al* 2006, Bowling *et al* 2010). In both land and atmospheric segments, the evaporative fraction (EF = LE/(LE + H), where LE and H are latent and sensible heat fluxes) is considered a central variable of interest (Koster *et al* 2009, Ford *et al* 2014, Feldman *et al* 2019), which defines how the land surface partitions net radiation into latent versus sensible heat fluxes.

Surface energy partitioning and land–atmosphere coupling are subject to land-surface characteristics (Koster *et al* 2004, Carleton *et al* 2008, Koster *et al* 2010) and can be affected by land-use and land-cover change (LULCC) (Cooley *et al* 2005, Hirsch *et al* 2014, Lorenz and Pitman 2014). As one of the major LULCC activities, deforestation breaks or at least weakens the existing linkage within the land-vegetation-atmosphere continuum, by removing woody plants that could potentially transpire a large amount of water into the atmosphere (Claussen *et al* 2001, Davin and de Noblet-ducoudré 2010, Myoung *et al* 2012). Consequently, the land surface tends to dissipate energy through the sensible heat pathway (Gash and Nobre 1997) rather than the

latent heat pathway in deforested versus forested land (Evaristo and McDonnell 2019). However, observed EF does not necessarily decline after deforestation, owing to the concurrent changes of albedo and surface energy balance (Luyssaert *et al* 2014). The separation of the compounding changes (vegetation cover and background atmospheric forcings) (Winckler *et al* 2017) is one of the major challenges in understanding how deforestation affects both land-surface energy partitioning and land–atmosphere coupling.

The patterns and controllers of EF have been widely investigated in the scientific literature (Brimelow *et al* 2011, Findell *et al* 2011). However, most of these studies have focused on the impacts related to soil states (i.e. soil moisture) (Ford *et al* 2014, Feldman *et al* 2019), while fewer studies have considered the role of vegetation cover and other factors (Myoung *et al* 2012, Williams *et al* 2016). This knowledge gap necessitates a comprehensive examination of how vegetation cover and other environmental states could potentially impact surface-energy partitioning before and after deforestation. A second challenge is to extend the analysis of the soil moisture–EF relationship (Dirmeyer 2011) to include relevant variables that could potentially drive surface-energy partitioning.

Linear correlative relationships have been widely used to analyze coupling between land states (i.e. soil moisture) and surface-energy partitioning (Basara and Crawford 2002, Ford *et al* 2014), even though nonlinearity in these interactions are acknowledged (Brubaker 1995, Zeng *et al* 2002). Therefore, linear-correlation-based representation of land–atmosphere coupling potentially leads to an incomplete understanding or misleading conclusions.

In this study, we analyze these nonlinearities and develop relevant metrics to quantify nonlinear impacts on surface-energy partitioning from deforestation. We diagnose the strength of land–atmosphere coupling using a recently synthesized FLUXNET dataset (Chen *et al* 2018) with paired forest-versus-non-forested land surfaces that share common climate forcing. Thus, differences in land–atmosphere coupling strength between paired forested and non-forested sites can be attributed to deforestation-induced land-cover change. We apply a novel and nonlinear metric (transfer entropy) based on information theory (Liu *et al* 2019) to diagnose how land-cover change (deforestation) affects EF and land–atmosphere coupling.

2. Methodology

2.1. Paired FLUXNET dataset

In this study, 29 pairs of FLUXNET sites from the FLUXNET2015 Tier 1 and AmeriFlux datasets (Baldocchi *et al* 2001) were used. The spatial locations of the paired sites are shown in figure 1, and the general information of the

sites are listed in table S1 (available online at stacks.iop.org/ERL/16/024014/mmedia). Each pair contains a forested (e.g. broadleaf or needleleaf forests) site and a nearby non-forest (e.g. grassland, cropland, or open shrub) site. The median linear distance between the paired sites is 21.6 km, and the median elevation difference is 20.0 m. Because of the proximities, we assume the two sites within each pair share similar atmospheric conditions. Although the meteorological measurements at the paired sites are not identical, Chen *et al* (2018) have demonstrated that the differences in meteorology are generally small and not likely a major factor in simulated surface flux differences in most of the pairs. Therefore, the difference (forest vs non-forest) in surface fluxes can be considered as the effects of deforestation.

Sensible (H) and latent (LE) heat fluxes (daily averaged fluxes from 10am to 4pm) are used to calculate the EF ($EF = LE/(LE + H)$) for both forested and non-forested sites, which serves as a target variable in the following transfer entropy analysis. The canopy photosynthesis flux (gross primary productivity (GPP)) is derived from the measured net ecosystem exchange (NEE) of CO_2 and total ecosystem respiration, the latter was extrapolated from the nighttime NEE using environmental variables (Reichstein *et al* 2005). We apply GPP as a proxy for vegetation dynamics and stomatal conductance (Williams and Torn 2015). In this study, we also include other available observations (from FLUXNET) in our analysis: downwelling shortwave radiation (R), temperature (T), precipitation (P), and VPD to investigate how atmospheric conditions affect EF. The analysis is conducted at relatively dry and wet sites, which are selected by their annual precipitation being either lower or higher than the mean of all the sites.

2.2. Transfer entropy analysis

To quantify directional control of a source variable (e.g. GPP) on a target variable (e.g. EF), information theory states that the uncertainty underlying the target variable could be significantly reduced, if it shares a significant amount of information entropy with the source variable, when excluding effects from confounders (Ruddell and Kumar 2009). Transfer entropy measures the amount of information from a source variable to a target variable. If significant transfer entropy exists, a causal link from a source variable to a target variable exists. Transfer entropy is based on Shannon information entropy (Shannon 1949), which measures the uncertainty of a system, and can be derived from the probability distribution of the variable:

$$H(X) = - \sum^p (x_t) \log_2 p(x_t) \quad (1)$$

where x_t is time series of variable X . To estimate the probabilities in equation (1), each variable is discretized into several fixed-interval histogram bins.

x_t , therefore, can also be regarded as values in the time series X for the t^{th} bin. $H(X)$ is measured in bits and hereafter will be referred as information entropy.

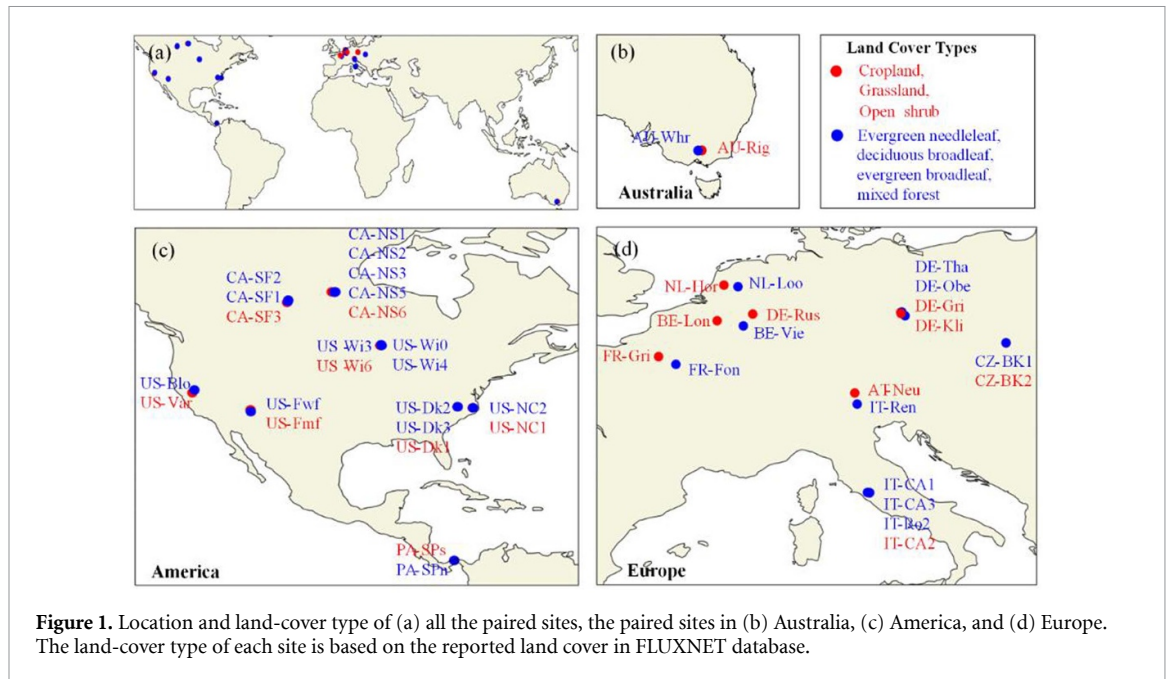
Transfer entropy measures the shared information entropy between source and target variables by excluding the information entropy from confounders. As increasing the number of confounders will cause high-dimensional computation and statistical reliability issues (Runge 2018, Runge *et al* 2019), we only consider the immediate history of a target variable as the confounder, which always contributes the most confounding information in many study cases (Ruddell and Kumar 2009). The transfer entropy from a source variable (X) to a target variable (Y), knowing the historical condition of target variable, is defined as (Schreiber 2000):

$$T(X \rightarrow Y) = \sum_{y_t, y_t^{[k]}, x_t^{[l]}} p(y_t, y_t^{[k]}, x_t^{[l]}) \times \log_2 \frac{p(y_t | (y_t^{[k]}, x_t^{[l]}))}{p(y_t | y_t^{[k]})} \quad (2)$$

where l and k are leading time of source variable X and the historical condition of Y , respectively and y_t are values in the Y time series for the t^{th} bin. In the experiments, we use daily data, and set k as 1 day (Ruddell and Kumar 2009). For the time lag, l , 0–5 days are considered, because we focus on short-term processes within a few days (Scott *et al* 1997, Brunel *et al* 2006, Ivanov *et al* 2008). For the binning parameter, we use 11 bins, according to the recommendation of the proper bin numbers from Ruddell and Kumar (2009).

The shuffled surrogate method (Kantz and Schürmann 1996) is employed to determine whether an information flow between coupling variables is significantly stronger than that between shuffled source and target time series by random chance. X_s and Y_s are obtained by shuffling X_t and Y_t randomly in time to destroy time correlations. Surrogate transfer entropy $T_s(X_s \rightarrow Y_s)$ is computed 100 times using Monte Carlo simulations. A one-tailed significance test is applied to determine the 95% confidence of the transfer entropy (Ruddell and Kumar 2009). The detailed key steps of significant test can be seen in text S1. Finally, relative transfer entropy (T/H) is calculated to normalize transfer entropy with its total uncertainty (Bossomaier *et al* 2016) and make the strengths of transfer entropy inferred from observations and E3SM land model (ELM) model simulations be comparable.

For each couple of variables (e.g. $T/H(X \rightarrow Y)$), we chose the maximum value of causal strength among all the time lags (0–5 days) to represent the strongest interactions within the 5-day time window. Comparison of the strongest causal links within a time window is also widely employed in



other causality detection researches (Ruddell and Kumar 2009, Ye *et al* 2015). To make sure all the selected causal links are significant, we conducted significant tests on each potential causal link at each time lag. For the potential causal links that failed to pass the significant test, their transfer entropy was set to zero. In this study, all the analysis is based on the time lags with peak strengths at which most information is transferred (Ruddell and Kumar 2009). We append details of the causal strengths at different time lags in the supplement (text S2, figure S4, tables S3 and S4).

2.3. Land surface model simulations

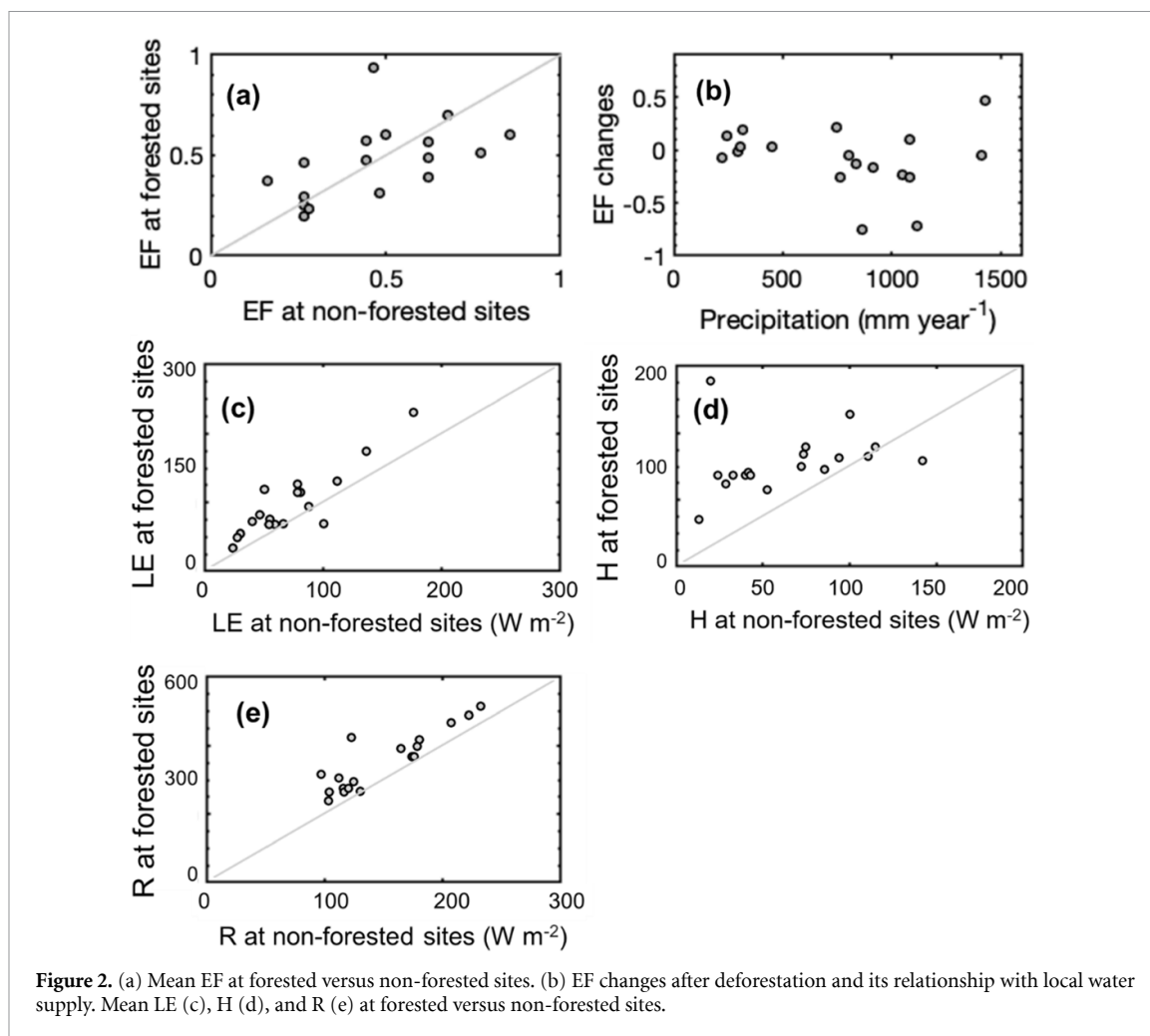
We use offline simulations of the land model (ELM) in the Energy, Exascale, and Earth System Model (E3SM) (Zhu *et al* 2019, 2020) forced with *in situ* climate at the paired sites to assess how well the observed patterns of surface energy partitioning are reproduced. Although the offline ELM does not simulate two-way feedbacks between the atmosphere and land surface, it is able to capture one-way causal links from the atmosphere to the land surface. Therefore, the ELM simulated causal controls from environmental factors to EF can be directly compared with those derived from observations. The ELM satellite phenology (SP) mode uses prescribed vegetation phenology (leaf area index) from the Moderate Resolution Imaging Spectroradiometer (MODIS) satellite and observed temperature, precipitation, downwelling shortwave and longwave radiation, and vapor-pressure deficit to prognostically simulate ecosystem carbon, water, and energy dynamics. The longitude and latitude of each site are used to extract necessary vegetation and soil properties from a global surface dataset (Koven *et al* 2013), including e.g.

global distribution of plant functional types (Friedl *et al* 2010), soil texture (Webb *et al* 2000), and parent material phosphorus content (Yang *et al* 2013). Before transient simulations, ELM model ran a 200-year accelerated spinup simulation to accumulate soil organic carbon and vegetation biomass. Then ELM ran another 200-year regular spinup to further stabilize the local hydrological and biogeochemical cycles, using the repeated 20 year (1901–1920) historical climate forcings at each site (Cai *et al* 2019).

3. Results and discussion

3.1. How deforestation changes the land-surface energy partitioning

First, we investigate the deforestation effects on land-surface energy partitioning between H and LE using the EF. Shifting from forested to non-forested open lands, we did not identify any consistent changes in observed EF (figure 2(a), table S7). In general, deforestation led to significantly decline in LE, H, and R (figures 2(c), (d) and (e), table S7), resulting in relatively small EF effects (table S7). Diurnal and seasonal dynamics of LE and H confirm that the decline of LE and H mainly occur during daytime and during summer, due to limited evapotranspiration and smaller net radiation inputs over non-forested surfaces (Chen *et al* 2018). Consequently, LE and H offset each other to either enhance or reduce EF (figure 2(a)). For the non-forested sites, the 25th, 50th, and 75th percentiles of EF were 0.37, 0.46, 0.59, respectively. Compared with the 25th, 50th, and 75th percentiles of EF at forested sites (0.27, 0.48, 0.75), deforestation tended to enhance EF when the forested EF was low, but, conversely, reduced EF when the forested EF was high (detailed pairwise comparison of



EF in forested and non-forested sites can be seen in figure S1). Similarly, across precipitation gradients from 0 to 1200 mm yr⁻¹ (figure 2(b)), the differences between forested and non-forested EF at the sites with precipitation from 600 to 1200 mm yr⁻¹ was significantly lower than those at the sites with precipitation lower than 600 mm yr⁻¹ (figure 2(b), text S3). It seems that the EF difference increased again when the mean precipitation higher than 1200 mm yr⁻¹ (figure 2(b)), but not enough data was available to test this hypothesis.

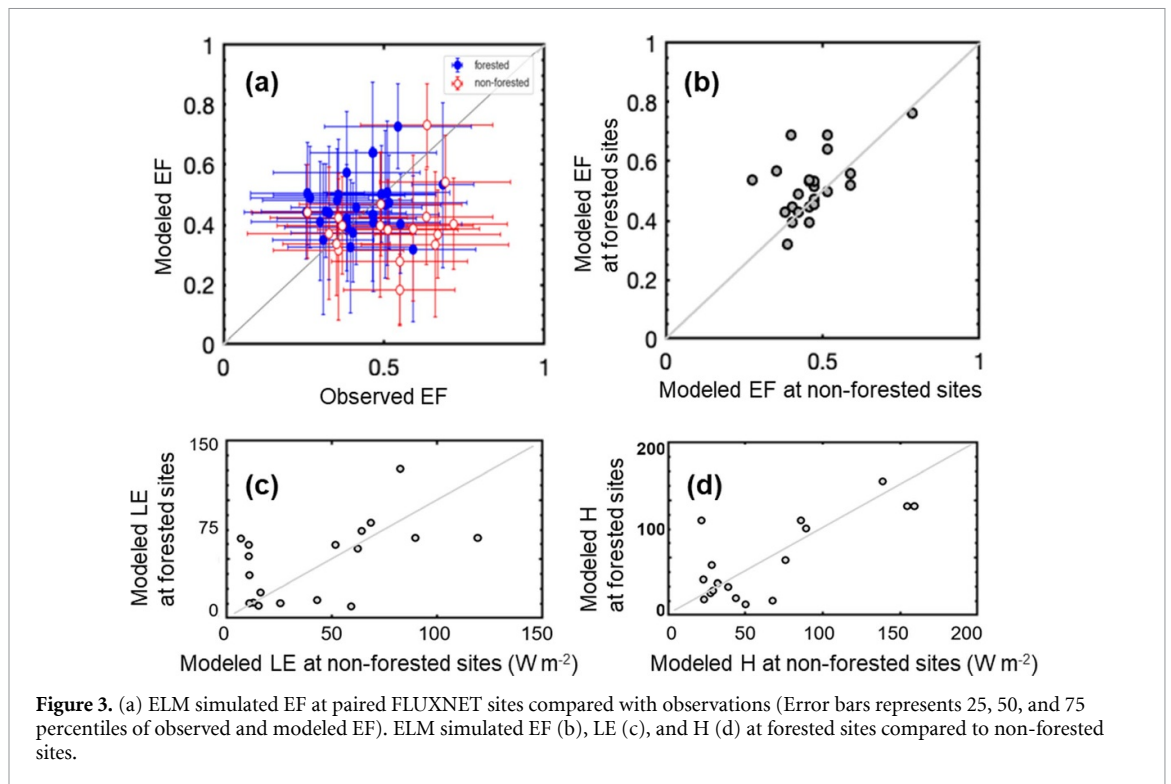
In general, ELM better reproduced observed EF at the forested sites than non-forested sites as the mean absolute error at forested sites was significantly lower than that of non-forest sites (table S5). Meanwhile, ELM tended to significantly underestimate EF at non-forested sites (figure 3(a) and table S6). Therefore, ELM better reproduced observed EF at the forested sites than non-forested sites. This inaccuracy was due to an underestimation of evapotranspiration and latent heat fluxes at some C3 grass and temperate shrub sites, particularly during spring and summer, as we identified in a recent study (Cai *et al* 2019). Similar to the observed forested and non-forested EF relationship (figure 2(a)), ELM also did not exhibit a systematic shift in surface-energy partitioning due to

forest cover change (figure 3(b)). But the ELM failed to represent the systematic shift of LE and H caused by deforestation (figures 3(c) and (d), table S8).

3.2. How deforestation affects land part of land–atmosphere coupling

Because of limited observations of soil moisture in the FLUXNET paired dataset, an investigation of the classic soil moisture–EF relationship (Dirmeyer 2011) is not considered here. Instead, vegetation controls over land–atmosphere coupling are evaluated by the relative transfer entropy from Gross Primary Production (GPP) to EF, taking GPP as a proxy for stomatal conductance that regulates water flow from soil to the atmosphere (Baldocchi *et al* 2001). Such an assumption is largely supported by the close relationship between observed GPP and evapotranspiration fluxes across a wide range of vegetation covers (Mu *et al* 2007, Gitelson *et al* 2014, Jiang and Ryu 2016).

The observed directional control of GPP on EF at forested sites was significantly higher than that at non-forested sites (figure 4(a), table S9), indicating a stronger vegetation impact on atmospheric conditions over forests through recycling and convective cloud development (Blyth *et al* 1994, Trenberth 1999, Freedman *et al* 2001). However, no statistically



significant difference was identified in ELM between forested and non-forested sites in terms of the directional control of GPP on EF (figure 4(b), table S9). ELM generally captured a similar directional control from GPP on EF at the non-forested sites (figures 4(a) and (b), dashed lines, table S10), but failed at the forested sites (figures 4(a) and (b), solid lines, table S10). Moreover, the results (figures 4(c) and (d), table S12) showed that at relatively dry sites (mean annual precipitation $<373 \text{ mm yr}^{-1}$, figure S2), the observed control from GPP on EF remained similar with that at relatively wet sites (mean annual precipitation $>373 \text{ mm yr}^{-1}$, figure S2). It demonstrates the important role of stomatal controls on ecosystem water loss through evapotranspiration in both relatively dryer and wetter conditions. Similar conclusions have been drawn from studies at U.S. Southern Great Plains sites, where the strong relationship between GPP and EF was observed during both relatively dry and wet periods (Williams and Torn 2015). However, the ELM significantly underestimated the control from GPP on EF at forested sites over relatively dry areas (figure 4(c), table S11). The underestimation was not significant at the forested sites over relative wet areas, as well as at the non-forested sites in both relatively dry and wet areas (figures 4(c) and (d), table S11).

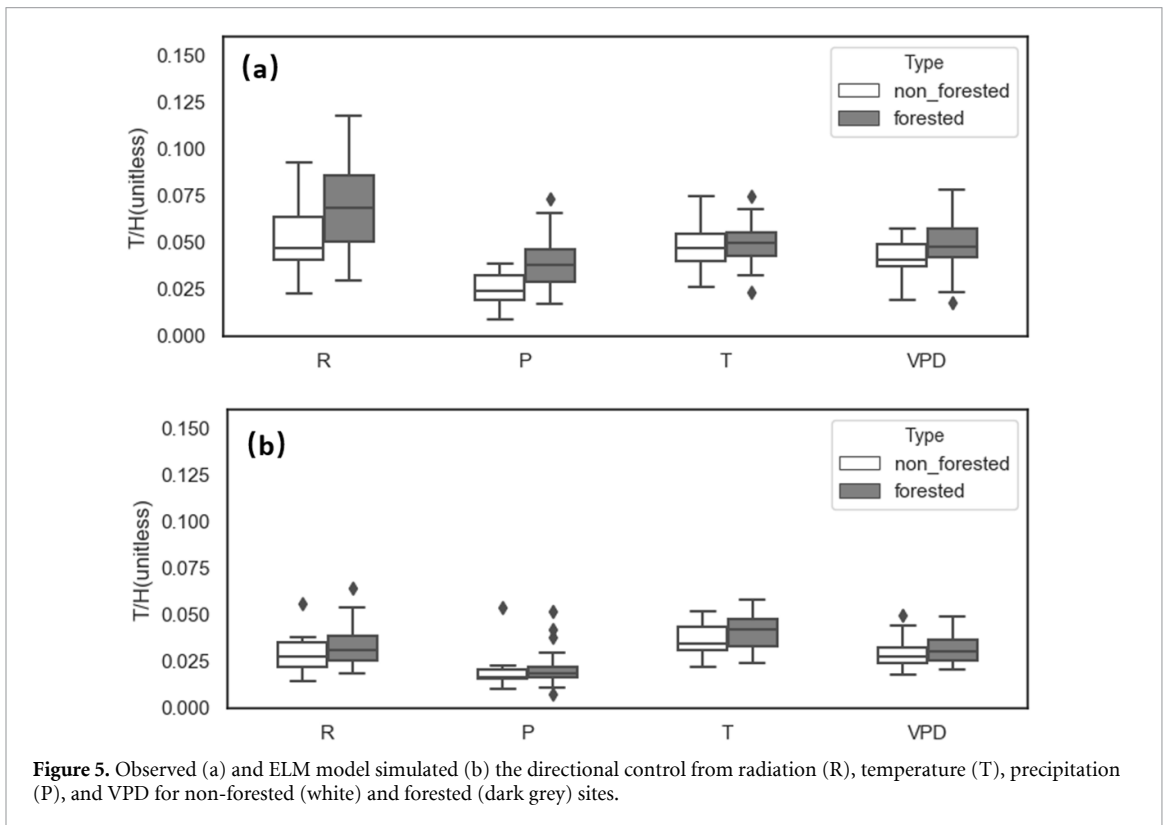
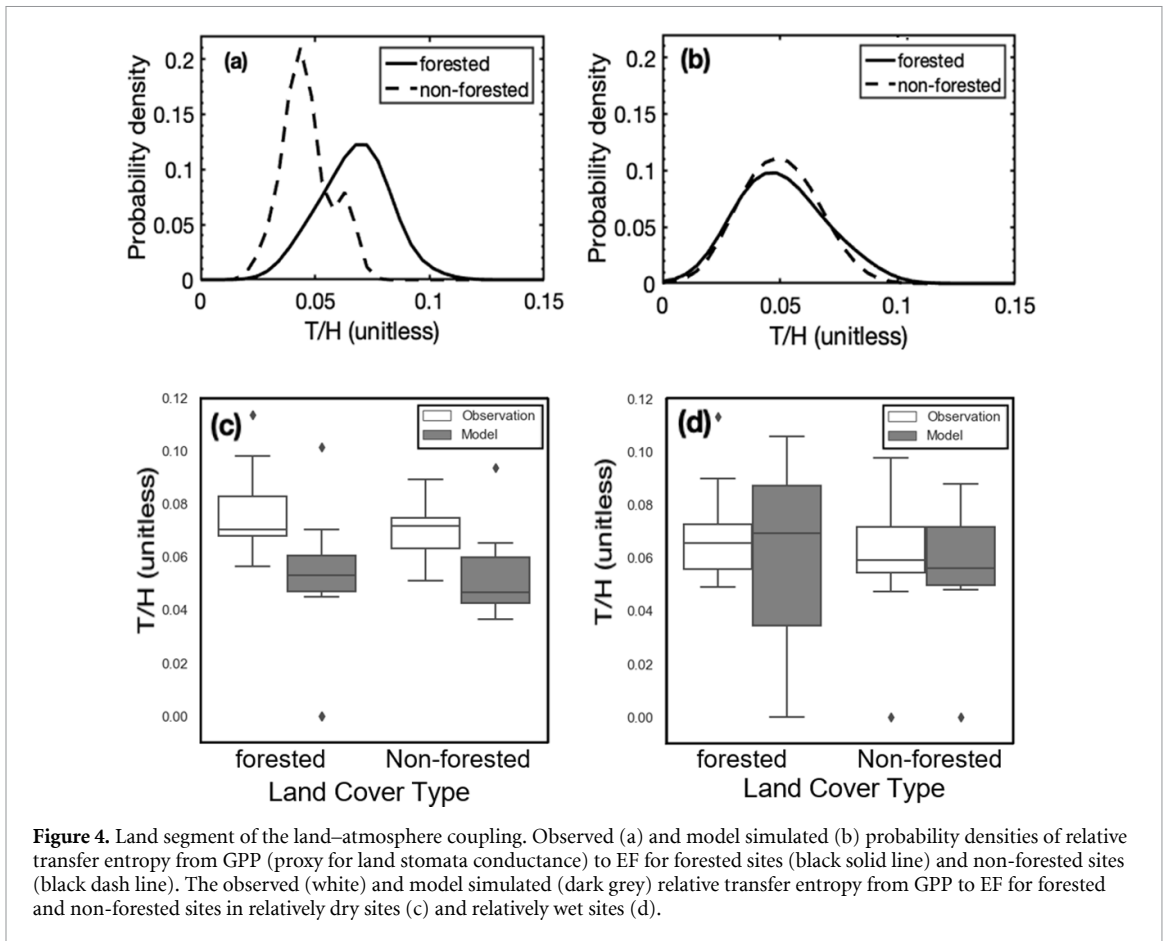
3.3. How deforestation affects atmosphere part of land–atmosphere coupling

Together with the controls from vegetation and soil, atmospheric conditions (i.e. temperature and radiation) are also expected to mediate

surface-energy partitioning, and consequently contribute to land–atmosphere coupling (Farah *et al* 2004, Peng *et al* 2018). For example, when the surface-water supply is abundant, higher solar radiation (a major source of surface energy) will potentially provide more energy to evaporate surface water and also affect plant stomatal behavior (Pieruschka *et al* 2010), exerting strong controls on latent heat flux (figure S3). Such controls, however, might weaken during dry periods, especially when the canopy is dense and plants actively close stomata to prevent water losses. In this case, removing vegetation cover might help couple the incoming radiation back again with soil evaporation and EF, even though the soil is relatively dry (Gentine *et al* 2007).

In the study, solar radiation (R) exerted a much stronger control on EF at forested sites (figure 5(a), table S13), with a mean causal strength 27%–44% larger than the controls from other drivers including temperature (T), precipitation (P), and VPD (figure 5(a), table S13). Deforestation tended to reduce the controls from R, and P on EF, and maintained the directional T, and VPD on EF (figure 5(a), table S14).

ELM model results revealed that although EF values at forested sites were relatively well simulated, the directional controls from R, P, T and VPD on EF were consistently underestimated (figures 5(a) versus (b), table S15). Moreover, the ELM-simulated land segment of land–atmosphere coupling was not sensitive to deforestation or changes in vegetation cover (table S16). The major discrepancy is in how available energy (solar radiation) reshapes the surface-energy partitioning before and after the forest is removed.



3.4. Implications for land-model development and analysis

Land-surface models have been used to analyze responses of land carbon, water, and energy dynamics to ongoing environmental changes (Zhu and Zhuang 2013, 2015, Riley *et al* 2018, Fleischer *et al* 2019, Medvigy *et al* 2019, Zhu *et al* 2019). LULCCs, such as deforestation, significantly disturb the vegetation cover and modify land-surface characteristics (Gash and Nobre 1997, Davin and de Noblet-ducoudré 2010), thus imposing critical challenges in evaluating land-surface model fidelity in terms of simulating carbon, water, and energy fluxes before and after deforestation (Lawrence *et al* 2016). Significant effort has been conducted to parameterize land-surface models and reduce the model-data discrepancy (Decharme 2007, Chen *et al* 2010, Domínguez *et al* 2010, Zhu *et al* 2016, Meier *et al* 2018, Cai *et al* 2019, Song *et al* 2020). However, it has not been fully investigated why model biases exist. This study expands benchmarking of land-surface energy-flux partitioning to include cause–effect relationships that might be responsible for model biases. We highlight potential model biases of leaf stomata conductance controls on surface-energy partitioning in the ELM model, especially when the land surface is forested, and the model’s significant underestimation of how incoming radiation and precipitation control surface-energy partitioning for both non-forested and forested land surfaces. In contrast, temperature and VPD are much more accurately represented in ELM in terms of their directional control on surface energy partitioning. Therefore, this analysis could direct future ELM model development to particularly focus on vegetation stomata conductance parameterization, radiation transfer, and precipitation partitioning (i.e. intercept, overflow) processes.

Analysis of deforestation effects on surface-energy partitioning is often complicated by compounding changes in vegetation cover and background climate forcings (Winckler *et al* 2017). Isolating the effects of these changes is challenging in observations but is valuable for improving understanding of how and why deforestation reshapes land-surface energy partitioning. This analysis applied a FLUXNET dataset in which non-forested and forested sites are paired with similar atmosphere conditions (e.g. temperature, precipitation) (Chen *et al* 2018). Thus, the diagnosed biases in the directional controls could be attributed to the processes that govern the directional controls rather than originating from differentness in background climate forcings.

4. Conclusion

Deforestation significantly modifies the land surface by changing vegetation cover, disturbing surface-energy partitioning, and land-atmosphere

interactions. In this study, we investigated the changes in land-surface energy partitioning with a FLUXNET dataset of paired forested and non-forested sites. We applied nonlinear diagnostic metrics to quantify how land and atmospheric states control surface-energy partitioning using transfer entropy calculations. We found that: (a) deforestation simultaneously reduces latent and sensible heat fluxes due to a reduction of both evapotranspiration and incoming radiation, thus possibly leading to either an increase or decrease in EF; (b) GPP exerted a strong control on the EF in forests and deforestation weakens this control; (c) incoming radiation was the most prominent atmospheric variable mediating the EF; (d) the ELM simulated the EF better at forested sites than non-forested sites; however, it failed to capture most of the directional controls from either land segment or atmosphere segment on surface-energy partitioning at both forested and non-forested sites. This study therefore highlights the need for benchmarking model-simulated directional controls on land-atmosphere water and energy fluxes to improve land-model performance.

Data availability statement

The data that support the findings of this study are available upon reasonable request from the authors.

Acknowledgments

This research was supported by the Reducing Uncertainties in Biogeochemical Interactions through Synthesis and Computation (RUBISCO) Scientific Focus Area and Energy Exascale Earth System Modeling (E3SM, <https://e3sm.org/>) Project, which are sponsored by the Earth and Environmental Systems Modeling (EESM) Program under the Office of Biological and Environmental Research of the US Department of Energy Office of Science. Lawrence Berkeley National Laboratory (LBNL) is managed by the University of California for the US Department of Energy under Contract No. DE-AC02-05CH11231. MC was supported by a Laboratory Directed Research and Development project sponsored by the Pacific Northwest National Laboratory of the US Department of Energy.

ORCID iDs

Kunxiaojuan Yuan  <https://orcid.org/0000-0002-1336-5768>

Qing Zhu  <https://orcid.org/0000-0003-2441-944X>

Lei Zhao  <https://orcid.org/0000-0002-6481-3786>

Xitian Cai  <https://orcid.org/0000-0002-4798-4954>

Fa Li  <https://orcid.org/0000-0002-0625-5587>

Liang Chen  <https://orcid.org/0000-0003-1553-2846>

References

- Allison S D and Treseder K K 2011 Climate change feedbacks to microbial decomposition in boreal soils *Fungal Ecol.* **4** 362–74
- Baldocchi D et al 2001 FLUXNET: a new tool to study the temporal and spatial variability of ecosystem-scale carbon dioxide, water vapor, and energy flux densities *Bull. Am. Meteorol. Soc.* **82** 2415–34
- Basara J B and Crawford K C 2002 Linear relationships between root-zone soil moisture and atmospheric processes in the planetary boundary layer *J. Geophys. Res. Atmos.* **107** ACL 10-11–ACL 10-18
- Blyth E, Dolman A and Noilhan J 1994 The effect of forest on mesoscale rainfall: an example from HAPEX-MOBILHY *J. Appl. Meteorol.* **33** 445–54
- Bossomaier T et al 2016 *An Introduction to Transfer Entropy* (Cham: Springer) pp 65–95
- Bowling D R, Bethers-Marchetti S, Lunch C K, Grote E E and Belnap J 2010 Carbon, water, and energy fluxes in a semiarid cold desert grassland during and following multiyear drought *J. Geophys. Res. Biogeosci.* **115** G04026
- Brimelow J C, Hanesiak J M and Burrows W R 2011 Impacts of land-atmosphere feedbacks on deep, moist convection on the Canadian Prairies *Earth Interact.* **15** 1–29
- Brubaker K L 1995 Nonlinear dynamics of water and energy balance in land-atmosphere interaction Massachusetts Institute of Technology (<http://hdl.handle.net/1721.1/36513>)
- Brunel J-P, Ihab J, Droubi A M and Samaan S 2006 Energy budget and actual evapotranspiration of an arid oasis ecosystem: Palmyra (Syria) *Agric. Water Manage.* **84** 213–20
- Cai X, Riley W J, Zhu Q, Tang J, Zeng Z, Bisht G and Randerson J T 2019 Improving representation of deforestation effects on evapotranspiration in the E3SM land model *J. Adv. Model. Earth Syst.* **11** 2412–27
- Carleton A M, Travis D J, Adegoke J O, Arnold D L and Curran S 2008 Synoptic circulation and land surface influences on convection in the Midwest US ‘Corn Belt’ during the summers of 1999 and 2000. Part II: role of vegetation boundaries *J. Clim.* **21** 3617–41
- Chen L, Dirmeyer P A, Guo Z and Schultz N M 2018 Pairing FLUXNET sites to validate model representations of land-use/land-cover change *Hydrol. Earth Syst. Sci.* **22** 111–25
- Chen Y, Yang K, Zhou D, Qin J and Guo X 2010 Improving the Noah land surface model in arid regions with an appropriate parameterization of the thermal roughness length *J. Hydrometeorol.* **11** 995–1006
- Claussen M, Brovkin V and Ganopolski A 2001 Biogeophysical versus biogeochemical feedbacks of large-scale land cover change *Geophys. Res. Lett.* **28** 1011–4
- Cooley H, Riley W J, Torn M S and He Y 2005 Impact of agricultural practice on regional climate in a coupled land surface mesoscale model *J. Geophys. Res. Atmos.* **110** D03113
- Davin E L and de Noblet-ducoudré N 2010 Climatic impact of global-scale deforestation: radiative versus nonradiative processes *J. Clim.* **23** 97–112
- Decharme B 2007 Influence of runoff parameterization on continental hydrology: comparison between the Noah and the ISBA land surface models *J. Geophys. Res. Atmos.* **112** D19108
- Dirmeyer P A 2011 The terrestrial segment of soil moisture–climate coupling *Geophys. Res. Lett.* **38** L16702
- Dominguez M, Gaertner M A, de Rosnay P and Losada T 2010 A regional climate model simulation over West Africa: parameterization tests and analysis of land-surface fields *Clim. Dyn.* **35** 249–65
- Evaristo J and McDonnell J J 2019 Global analysis of streamflow response to forest management *Nature* **570** 455–61
- Farah H, Bastiaanssen W and Feddes R 2004 Evaluation of the temporal variability of the evaporative fraction in a tropical watershed *Int. J. Appl. Earth Obs. Geoinf.* **5** 129–40
- Feldman A F, Short Gianotti D J, Trigo I F, Salvucci G D and Entekhabi D 2019 Satellite-based assessment of land surface energy partitioning–soil moisture relationships and effects of confounding variables *Water Resour. Res.* **55** 10657–77
- Findell K L et al 2011 Probability of afternoon precipitation in eastern United States and Mexico enhanced by high evaporation *Nat. Geosci.* **4** 434–9
- Fleischer K et al 2019 Amazon forest response to CO₂ fertilization dependent on plant phosphorus acquisition *Nat. Geosci.* **12** 736–41
- Ford T W, Wulff C O and Quiring S M 2014 Assessment of observed and model-derived soil moisture–evaporative fraction relationships over the United States Southern Great Plains *J. Geophys. Res. Atmos.* **119** 6279–91
- Freedman J M, Fitzjarrald D R, Moore K E and Sakai R K 2001 Boundary layer clouds and vegetation–atmosphere feedbacks *J. Clim.* **14** 180–97
- Friedl M A, Sulla-Menashe D, Tan B, Schneider A, Ramankutty N, Sibley A and Huang X 2010 MODIS collection 5 global land cover: algorithm refinements and characterization of new datasets *Remote Sens. Environ.* **114** 168–82
- Gash J and Nobre C 1997 Climatic effects of Amazonian deforestation: some results from ABRACOS *Bull. Am. Meteorol. Soc.* **78** 823–30
- Gentine P, Entekhabi D, Chehbouni A, Boulet G and Duchemin B 2007 Analysis of evaporative fraction diurnal behaviour *Agric. For. Meteorol.* **143** 13–29
- Gentine P, Green J K, Guérin M, Humphrey V, Seneviratne S I, Zhang Y and Zhou S 2019 Coupling between the terrestrial carbon and water cycles—a review *Environ. Res. Lett.* **14** 083003
- Gitelson A A, Peng Y, Arkebauer T J and Schepers J 2014 Relationships between gross primary production, green LAI, and canopy chlorophyll content in maize: implications for remote sensing of primary production *Remote Sens. Environ.* **144** 65–72
- Guo Z et al 2006 GLACE: the global land–atmosphere coupling experiment. Part II: analysis *J. Hydrometeorol.* **7** 611–25
- Hirsch A, Pitman A and Kala J 2014 The role of land cover change in modulating the soil moisture–temperature land–atmosphere coupling strength over Australia *Geophys. Res. Lett.* **41** 5883–90
- Ivanov V Y, Bras R L and Vivoni E R 2008 Vegetation–hydrology dynamics in complex terrain of semiarid areas: 1. A mechanistic approach to modeling dynamic feedbacks *Water Resour. Res.* **44** W03429
- Jiang C and Ryu Y 2016 Multi-scale evaluation of global gross primary productivity and evapotranspiration products derived from breathing Earth system simulator (BESS) *Remote Sens. Environ.* **186** 528–47
- Kantz H and Schürmann T 1996 Enlarged scaling ranges for the KS-entropy and the information dimension *Chaos* **6** 167–71
- Koster R D et al 2004 Regions of strong coupling between soil moisture and precipitation *Science* **305** 1138–40
- Koster R D et al 2010 Contribution of land surface initialization to subseasonal forecast skill: first results from a multi-model experiment *Geophys. Res. Lett.* **37** L02402
- Koster R, Schubert S and Suarez M 2009 Analyzing the concurrence of meteorological droughts and warm periods, with implications for the determination of evaporative regime *J. Clim.* **22** 3331–41
- Koven C D, Riley W J, Subin Z M, Tang J Y, Torn M S, Collins W D, Bonan G B, Lawrence D M and Swenson S C 2013 The effect of vertically resolved soil biogeochemistry and alternate soil C and N models on C dynamics of CLM4 *Biogeosciences* **10** 7109–31
- Kukul M and Irmak S 2016 Long-term patterns of air temperatures, daily temperature range, precipitation, grass-reference evapotranspiration and aridity index in the USA Great Plains: part II. Temporal trends *J. Hydrol.* **542** 978–1001

- Lawrence D M *et al* 2016 The land use model intercomparison project (LUMIP) contribution to CMIP6: rationale and experimental design *Geosci. Model Dev.* **9** 2973–98
- Lei H, Yang D, Lokupitiya E and Shen Y 2010 Coupling land surface and crop growth models for predicting evapotranspiration and carbon exchange in wheat-maize rotation croplands *Biogeosciences* **7** 3363–75
- Liu B Y *et al* 2019 Using information theory to evaluate directional precipitation interactions over the West Sahel region in observations and models *J. Geophys. Res. Atmos.* **124** 1463–73
- Lombardozzi D L, Bonan G B, Smith N G, Dukes J S and Fisher R A 2015 Temperature acclimation of photosynthesis and respiration: a key uncertainty in the carbon cycle-climate feedback *Geophys. Res. Lett.* **42** 8624–31
- Lorenz R and Pitman A J 2014 Effect of land-atmosphere coupling strength on impacts from Amazonian deforestation *Geophys. Res. Lett.* **41** 5987–95
- Luyssaert S *et al* 2014 Land management and land-cover change have impacts of similar magnitude on surface temperature *Nat. Clim. Change* **4** 389–93
- Medvigy D, Wang G, Zhu Q, Riley W J, Trierweiler A M, Waring B, Xu X and Powers J S 2019 Observed variation in soil properties can drive large variation in modelled forest functioning and composition during tropical forest secondary succession *New Phytol.* **223** 1820–33
- Meier R, Davin E L, Lejeune Q, Hauser M, Li Y, Martens B, Schultz N M, Sterling S and Thiery W 2018 Evaluating and improving the community land model's sensitivity to land cover *Biogeosciences* **15** 4731–57
- Mu Q, Heinsch F A, Zhao M and Running S W 2007 Development of a global evapotranspiration algorithm based on MODIS and global meteorology data *Remote Sens. Environ.* **111** 519–36
- Myoung B, Choi Y-S, Choi S-J and Park S K 2012 Impact of vegetation on land-atmosphere coupling strength and its implication for desertification mitigation over East Asia *J. Geophys. Res. Atmos.* **117** D12113
- Peng L, Li D and Sheffield J 2018 Drivers of variability in atmospheric evaporative demand: multiscale spectral analysis based on observations and physically based modeling *Water Resour. Res.* **54** 3510–29
- Pieruschka R, Huber G and Berry J A 2010 Control of transpiration by radiation *Proc. Natl Acad. Sci.* **107** 13372–7
- Puma M J, Koster R D and Cook B I 2013 Phenological versus meteorological controls on land-atmosphere water and carbon fluxes *J. Geophys. Res. Biogeosci.* **118** 14–29
- Reichstein M *et al* 2005 On the separation of net ecosystem exchange into assimilation and ecosystem respiration: review and improved algorithm *Glob. Change Biol.* **11** 1424–39
- Riley W J, Zhu Q and Tang J 2018 Weaker land-climate feedbacks from nutrient uptake during photosynthesis-inactive periods *Nat. Clim. Change* **8** 1002
- Ruddell B L and Kumar P 2009 Ecohydrologic process networks: 1. Identification *Water Resour. Res.* **45** W03419
- Runge J 2018 Causal network reconstruction from time series: from theoretical assumptions to practical estimation *Chaos* **28** 075310
- Runge J *et al* 2019 Inferring causation from time series in Earth system sciences *Nat. Commun.* **10** 1–13
- Santanello J A Jr, Peters-Lidard C D, Kennedy A and Kumar S V 2013 Diagnosing the nature of land-atmosphere coupling: a case study of dry/wet extremes in the US Southern Great Plains *J. Hydrometeorol.* **14** 3–24
- Schreiber T 2000 Measuring information transfer *Phys. Rev. Lett.* **85** 461
- Scott R, Entekhabi D, Koster R and Suarez M 1997 Timescales of land surface evapotranspiration response *J. Clim.* **10** 559–66
- Shannon C E 1949 Communication theory of secrecy systems *Bell Syst. Tech. J.* **28** 656–715
- Song J, Miller G R, Cahill A T, Aparecido L M T and Moore G W 2020 Modeling land surface processes over a mountainous rainforest in Costa Rica using CLM4. 5 and CLM5 *Geosci. Model Dev.* **13** 5147–73
- Suyker A E and Verma S B 2010 Coupling of carbon dioxide and water vapor exchanges of irrigated and rainfed maize-soybean cropping systems and water productivity *Agric. For. Meteorol.* **150** 553–63
- Trenberth K E 1999 Atmospheric moisture recycling: role of advection and local evaporation *J. Clim.* **12** 1368–81
- Webb R, Rosenzweig C and Levine E 2000 Global soil texture and derived water-holding capacities (Oak Ridge National Laboratory Distributed Active Archive Center) (available at: http://daac.ornl.gov/cgi-bin/dsviewer.pl?ds_id=548)
- Williams I N *et al* 2016 Land-atmosphere coupling and climate prediction over the US Southern Great Plains *J. Geophys. Res. Atmos.* **121** 12125–44
- Williams I N and Torn M S 2015 Vegetation controls on surface heat flux partitioning, and land-atmosphere coupling *Geophys. Res. Lett.* **42** 9416–24
- Winckler J, Reick C H and Pongratz J 2017 Robust identification of local biogeophysical effects of land-cover change in a global climate model *J. Clim.* **30** 1159–76
- Yang X, Post W M, Thornton P E and Jain A 2013 The distribution of soil phosphorus for global biogeochemical modeling *Biogeosciences* **10** 2525–37
- Ye H, Deyle E R, Gilarranz L J and Sugihara G 2015 Distinguishing time-delayed causal interactions using convergent cross mapping *Sci. Rep.* **5** 14750
- Zeng N, Hales K and Neelin J D 2002 Nonlinear dynamics in a coupled vegetation-atmosphere system and implications for desert-forest gradient *J. Clim.* **15** 3474–87
- Zhang Q *et al* 2014 The hysteretic evapotranspiration-vapor pressure deficit relation *J. Geophys. Res. Biogeosci.* **119** 125–40
- Zhou S, Yu B, Huang Y and Wang G 2014 The effect of vapor pressure deficit on water use efficiency at the subdaily time scale *Geophys. Res. Lett.* **41** 5005–13
- Zhu Q, Riley W J, Iversen C M and Kattge J 2020 Assessing impacts of plant stoichiometric traits on terrestrial ecosystem carbon accumulation using the E3SM land model *J. Adv. Model. Earth Syst.* **12** e2019MS001841
- Zhu Q, Riley W J, Tang J, Collier N, Hoffman F M, Yang X and Bisht G 2019 Representing nitrogen, phosphorus, and carbon interactions in the E3SM land model: development and global benchmarking *J. Adv. Model. Earth Syst.* **11** 2238–58
- Zhu Q, Riley W J, Tang J and Koven C D 2016 Multiple soil nutrient competition between plants, microbes, and mineral surfaces: model development, parameterization, and example applications in several tropical forests *Biogeosciences* **13** 341–63
- Zhu Q and Zhuang Q 2013 Improving the quantification of terrestrial ecosystem carbon dynamics over the United States using an adjoint method *Ecosphere* **4** 118–38
- Zhu Q and Zhuang Q 2015 Ecosystem biogeochemistry model parameterization: do more flux data result in a better model in predicting carbon flux? *Ecosphere* **6** 1–20